Radiative muon absorption in calcium

A. Frischknecht,* W. Stehling,† G. Strassner,‡ and P. Truöl
Physik-Institut der Universität Zürich, 8001 Zürich, Switzerland

J. C. Alder,§ C. Joseph, J. F. Loude, J. P. Perroud, D. Ruegger, and T. M. Tran
Institut de Physique Nucléaire, Université de Lausanne, 1015 Lausanne, Switzerland

W. Dahme, H. Panke,** and R. Kopp
Sektion Physik, Universität München, 8046 Garching, Federal Republic of Germany
(Received 16 April 1985)

The photon spectrum from radiative absorption of negative muons in ^{40}Ca has been measured with a high-resolution pair spectrometer. The data are analyzed in order to determine the induced pseudoscalar coupling constant g_p in nuclear matter. When compared to models which use a realistic nuclear response function and avoid the closure approximation, a value of $g_p/g_A = 4.0 \pm 1.5$ is obtained, which indicates a quenching of this coupling compared to the nucleonic value by a factor 0.57 ± 0.25.

I. INTRODUCTION

For ordinary muon capture, once considered a testing ground for the parameters of the semileptonic weak interaction, the interest has shifted to nuclear structure aspects. The transition operator is thought to be sufficiently well understood, that one may test different nuclear model wave functions against a measured transition rate.[1] For the rare muon absorption process $(\mu^-,\nu_\mu\gamma)$, however, the original motivation for investigating muon capture still persists, since a particularly elusive part of the muon-nucleon interaction, the induced pseudoscalar coupling mediated by one-pion exchange, plays an important role here. While contributing negligibly to β decay and little to ordinary muon capture the induced pseudoscalar coupling influences strongly the photon spectrum and the absolute rate for the radiative absorption mode. This was realized first for the elementary process $\mu^-\mathrm{p}\rightarrow\mathrm{n}\nu_\mu\gamma$,[2] but the low rate has so far prohibited an experimental observation of this process. However, as was first demonstrated by Rood and Tolhoek,[3] the sensitivity prevails for capture on complex nuclei and the doubly closed shell nucleus ^{40}Ca has emerged as the standard experimental and theoretical laboratory for testing these ideas.

The present information on the induced pseudoscalar coupling constant g_p (at $q^2 = -0.88m_\mu^2$) and on radiative muon capture experiments can be quickly summarized, since previous work is not extensive. From the latest work on the orthomolecular capture rate for muonic hydrogen[4] one extracts $g_p = (7.0 \pm 1.5)g_A$. This value compares favorably with $g_p = (10.0 \pm 2.5)g_A$ derived from the β decay and muon capture rate of the ^{16}N($J^\pi = 0^-$, $E_x = 0.12$ MeV) to ^{16}O(g.s.) transition[5] and with $g_p = (9.0 \pm 1.7)g_A$ obtained from the recoil polarization and the capture rate of the ^{12}C(g.s.) to ^{12}B(g.s.) transition.[6] Within the limited precision all values agree with the theoretical expectation $g_p = 6.78g_A$, which is computed with the hypothesis of partially conserved axial vector current and pion-pole dominance (see, e.g., Wolfenstein[7]).

The three previous measurements of the ^{40}Ca$(\mu^-,\nu_\mu\gamma)$ photon spectrum[8–10] are displayed in Fig. 1. For experimental reasons, which are discussed below, only the spectrum above 57 MeV is measurable. The accuracy of the data reflects the principal difficulties of radiative muon capture experiments, the low yield (the radiative branch contributes only 2×10^{-5} to the total muon absorption

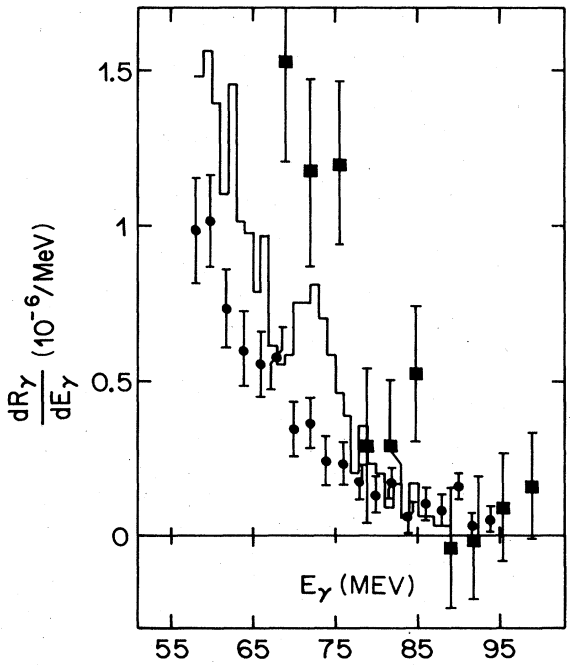

FIG. 1. Radiative muon capture photon spectra from previous experiments: ■, Ref. 8, 430 events total, $\Delta E/E = 17\%$; ●, Ref. 9, 4500 events total, $\Delta E/E = 16\%$; histogram Ref. 10, 1230 events total, $\Delta E/E = 29\%$. (R_γ is the ratio of the radiative to the ordinary muon capture rate.)

rate) the modest resolution attainable for photons between 50 and 100 MeV energy (between 16% and 29% FWHM was obtained with NaI spectrometers), and the high background environment from high-energy neutrons. Only the latest experiment[10] was able to overcome completely the latter problem and a value of $g_p=(6.5\pm1.6)g_A$ was extracted from the measured rate. This rate is, as we will show below, confirmed by the experiment reported here.

Though the apparent precision on g_p from $(\mu^-,\nu_\mu\gamma)$ experiments is comparable to that of other experiments, some reservations have to be made concerning its interpretation. In radiative muon absorption we are dealing with an inclusive process, and all the possible final states of the ^{40}K system, bound or unbound, can contribute. Consequently the theoretical spectrum, which is compared to the data, is not only sensitive to the parameters of the Hamiltonian, which we are interested in, but also to the nuclear model used to describe the initial ^{40}Ca ground state and the final ^{40}K energy levels. Most early calculations,[3,11–14] in particular those used in comparison with previous experiments, rely on the closure approximation, where the total transition strength is taken at a single mean energy. The maximum photon energy $k_{\max}$, which corresponds to this excitation energy, enters as a second free parameter, if theory and experiment are compared. Since the rate varies as $k_{\max}^6$, the two parameters $k_{\max}$ and g_p are strongly correlated in a low resolution experiment, where primarily the rate is measured.

As pointed out by Christillin *et al.*,[15,16] the closure approximation should also be critically examined on purely theoretical grounds, simply because the closure sum includes states of the nuclear excitation spectrum, which are energetically forbidden to contribute for high-energy photons. With increasing photon energy the allowed part of the excitation spectrum shrinks. Therefore all closure-type calculations overestimate the experimental rate or lead to highly improbable, negative values of g_p/g_A except for one calculation,[11] which was used to obtain the value of g_p quoted above. In this latter work, however, a large reduction of the rate due to a modification of the bound muon propagator was reached, which could not be reproduced in later calculations.[17] All complications with the closure approximation are avoided, if a nuclear response function dependent both on excitation energy and momentum transfer is used[16] or if in a shell model calculation all partial transitions are summed.[18,19]

When we started our experiments these microscopic calculations were in progress. This provided part of the motivation. The main incentive, however, was an experimental one. We had built and successfully operated with radiative pion capture reactions a high-resolution, neutron-insensitive photon detector—a pair spectrometer—for energies up to 250 MeV. The big advance in muon fluxes at the Swiss Institute for Nuclear Research meson factory allowed a measurement of such a low yield reaction as radiative muon capture even with a low acceptance detector with higher statistical accuracy than previous work. With an energy resolution of 1.5% (FWHM) an unfolded spectrum can be presented with absolute energy calibration, which puts for the first time radiative muon capture results on firm ground and hopefully will stimulate further refinements of theoretical calculations, especially in the direction of tracing the origin of the apparent quenching of the induced pseudoscalar coupling, which results when our data are analyzed with the models of Christillin[16] and Gmitro *et al.*[19]

We will discuss the implications of our results further in detail in the last section, after giving a rather thorough account of our experimental procedures. We feel forced by the troublesome history of radiative muon capture experiments to expose all problems we encountered and their solutions, if found, at length.

II. EXPERIMENTAL METHOD

A. Muon beam and detector system

In our experiment we made use of the most intense muon beam available at the isochronous proton synchrocylotron of the Swiss Institute of Nuclear Research (SIN). In this beam line ($\mu E1$) pions with a momentum of 220 MeV/c are accepted at forward angles from the ^{9}Be production target, bent into a superconducting solenoid with a 5 T magnetic field, which serves as the decay section, and finally a muon beam with a momentum of 125 MeV/c is focused onto the experimental target (Fig. 2). At a proton current of 100 μA this beam can deliver a muon intensity up to 30 MHz into an area of 24 cm^2.[20] The length of our spectrometer required a target position 2 m downstream from the best focal point for this beam. During our experiment the current of the SIN accelerator reached only 20 to 40 μA. Consequently, typical muon intensities available for our experiment were limited to 5 MHz into an area of 7×7 cm^2. After suitable degradation 80% of this beam could be brought to rest in either one of two metallic ^{40}Ca target configurations used:

(i) plates with volume $11\times9\times4$ cm^3 and surface density 7 g/cm^2,

(ii) grains with volume $10\times10\times10$ cm^3 and surface density 10 g/cm^2.

Both targets were packed into thin, sealed containers of surface density less than 0.1 g/m^2. The muons were distributed in time into 3.5 nsec wide bunches arriving with 20 nsec separation due to the 50 MHz radiofrequency of the SIN accelerator. The (estimated) electron contamination was 1%, while we deduced a pion contamination of $(1.3\pm0.2)\times10^{-3}$ from the prompt high energy part of our spectrum (see below).

The arrangement of muon and photon detectors is sketched in Fig. 2. The incoming flux was primarily measured with the last scintillation detector (μ_3) in front of the target. Its efficiency could be monitored comparing the coincidence rate of counters μ_2, μ_3, and μ_5 to that of μ_2 and μ_5. The size of the latter scintillator was chosen such that it intercepted only a small fraction of the beam passing through detector μ_3. The last scintillation counter in the beam, μ_4, was used only to determine the fraction of muons stopping in the target. It was removed during data taking at high intensities to eliminate a potential background source. Contributions to the nontarget associated background were eliminated mainly by local lead shielding blocks, as apparent from Fig. 2. The two major

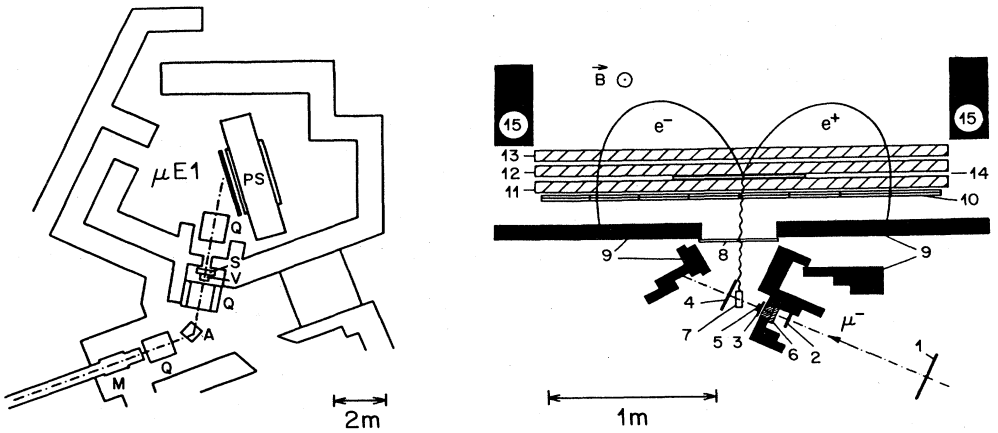

FIG. 2. The experimental setup. Left: Top view of second half of muon beam and experimental area with the pair spectrometer. *Q*: quadrupoles, *S*: slits, *V*: channel blocker, *M*: superconducting solenoid, *PS*: pair spectrometer. Right: Cross section through beam detectors and pair spectrometer. 1—5: Scintillation counters ($\mu_1-\mu_5$), 6: polyethylene degrader, 7: calcium target, 8: charged particle veto counter (scintillator), 9: lead shielding, 10: trigger counters (A_i,B_i) (scintillator), 11—13: multiwire proportional chambers, 14: gold/lead converter and converter chamber, 15: magnet return yoke.

sources were the muon beam dump and the degrader. All muons, which passed the lead collimator, had to pass also counter μ_3 ($10\times10\times0.3$ cm^3). This is an important requirement, since the beam telescope could not be part of the trigger, because during the muon lifetime of 340 nsec in ^{40}Ca on the average 1.7 muons were found in the target.

The photons were detected in a pair spectrometer. Since the properties of this detector have been described in detail elsewhere,[21] we give only its most salient features here and concentrate on those aspects different from the standard configuration.

Photons entered the spectrometer through a hole in a lead shielding wall with a solid angle of 1.9%. This hole was covered with two scintillation counters (AC) which vetoed charged particles. A thin, one-gap multiwire proportional chamber was sandwiched between two thin foils to convert photons into electron positron pairs. We used two different configurations of converters. In most of the runs two 88 μm gold foils (2.6% radiation length each) were mounted on each side of the chamber. A smaller data sample was taken with a 600 μm lead foil (11% radiation length) on one side and a 176 μm gold foil on the other side. The converter chamber allowed to distinguish those events originating in the first converter from those created in the second, and therefore to correct for the average energy loss in the second converter. This correction was only made for the two thicker converters. The electron-positron pair was bent in the 0.6 T magnetic field by 180°. The entrance and exit trajectories of the pairs were registered in three large multiwire proportional chambers (MWPC, active area 212×48 cm^2). Finally a double row of eight scintillation counters (A_i, B_i, $i=1,8$) signaled the arrival of a pair.

The transfer of the wire chamber information to CAMAC and magnetic tape via a PDP 11/40 computer was initiated, whenever the following trigger condition was fulfilled:

$$\text{Trigger}=(A_iB_i)\times(A_jB_j)\times\overline{\text{AC}}\times\text{FOR};\quad i\neq j,j\pm1\ .$$

The FOR requirement in the above trigger referred to a fast signal derived from the multiwire chambers. We require two hits in at least two of the three planes in both chambers behind the converter. This requirement was turned off for some runs to confirm that no good events were lost in using the FOR information. Those events, which occurred within 20 nsec after the arrival of a beam particle, were labeled prompt triggers on the data tape. With the lead-gold converter arrangement and an incoming muon rate of 5 MHz typical rates were AB_{ij}: 385 sec^{-1}, $AB_{ij}\times\overline{\text{AC}}$ (neutrals): 63 sec^{-1}, trigger (hardware photon candidates): 10 sec^{-1}, events on tape (photon candidates): 6.5 sec^{-1}. After off line pattern recognition the reconstructed photon rate reducted to 0.08 sec^{-1}. The majority (98.5%) of the taped events originated from either one of the following background sources: μ-decay electrons not vetoed by the charged particle anticounter or photons converted in the edges of lead collimator. Both types of events showed only a single charged particle track or sometimes, if both the electron and the positron had sufficient energy to exit from the collimator, two tracks with large spatial separation in the first and the second chamber. These events were easily distinguished from the photons converting in the converter foils, which showed no tracks in the center of the first chamber and two closely spaced tracks in the center of the second chamber. The remainder of the nonreconstructable events arose from random triggers (e.g., showers in different parts of spectrometer) or genuine pairs, where one of the members was hitting the chamber frames, but still triggers the counters. All these types of events were easily rejected by the pattern recognition program (see also Ref. 21).

High energy neutrons could only contribute to the trigger if they produced a knock-on proton in the first layer of trigger counters. If the proton had sufficient energy to pass through the second trigger layer, but small enough momentum to be bent in the spectrometer by 180°, it might be electronically registered, but only one track appeared in the chambers. Thus the pair spectrometer was completely insensitive to neutrons.

B. Calibration procedures

The standard method to obtain the line shape and acceptance for monoenergetic photons relies on the radiative pion capture reaction in hydrogen. The reaction $\pi^-p\rightarrow n\gamma$ occurring with 39.5% probability[22] yields monoenergetic photons with an energy of 129.4 MeV. The reaction $\pi^-p\rightarrow\pi^0n$ with a subsequent decay of the π^0 into two photons yields a continuous energy spectrum between 55 and 83 MeV. Before and after the experiment in the muon area we have calibrated the pair spectrometer using a liquid hydrogen target in the πE 1-pion channel of SIN. This calibration procedure was described previously in detail.[21] Three aspects were, however, different in the μ-capture application: (i) Different converter configurations were used. (ii) The magnetic field was lower (0.6 T instead of 0.8 T). (iii) Since photons down to an energy of 40 MeV were detected, the line shape could no longer be assumed to be constant for the energy region of interest. For radiative pion capture all interesting transitions occur between 100 and 130 MeV photon energy, where the line shape is nearly independent of energy.

Apart from measurements with a field of 0.8 T, which confirmed our published results, we measured for both converter configurations the photon spectrum from hydrogen at 0.6 T. The three spectra are shown in Fig. 3. We summed the contributions from both 88 μm gold converters (i.e., did not make use of the converter chamber information) and treated the 176 μm gold and 600 μm lead converter separately. Three quantities are of interest in the analysis of these data, the relative acceptance as a function of the photon energy, the absolute acceptance at the calibration energy, and the resolution as a function of energy. These three quantities were determined from a fit to the spectra of Fig. 3 in the following way. The expected photon spectrum can be expressed as

$$T(E_\gamma)=\frac{2P}{28}[\Theta(E_\gamma-55)-\Theta(E_\gamma-83)]+\delta(E_\gamma-129.4)\ ,$$

where energies are given in MeV, P is the Panofsky ratio $[P=\sigma(\pi^-p\rightarrow\pi^0n)/\sigma(\pi^-p\rightarrow n\gamma)=1.53$ (Ref. 22)] and Θ is the step function. This expression is multiplied with the relative acceptance $A_{\rm rel}(E'_\gamma)$ and folded with the resolution function $R(E'_\gamma,E'_\gamma-E_\gamma)$ and then compared to the data, i.e., the spectrum is fit with the function

$$S(E_\gamma)=N_0\int T(E'_\gamma)A_{\rm rel}(E'_\gamma)R(E'_\gamma,E'_\gamma-E_\gamma)dE'_\gamma\ .$$

The resolution is characterized by a superposition of a Gaussian distribution given by the energy loss due to ionization, the multiple scattering, the spatial resolution, the accuracy of the field map, the approximations used in the analysis of the chamber data, and a low energy tail arising from radiation energy losses. We chose the following parametrization:

$$E'_\gamma>E_\gamma-\Delta E,\quad R=N\exp(-y_0)\ ,$$

$$E'_\gamma\le E_\gamma-\Delta E,\quad R=N\sum_{i=0}^{3}c_i\exp(-y_i)/\sum_{i=0}^{3}c_i\ ,$$

with

$$\int R(E'_\gamma,E'_\gamma-E_\gamma)dE'_\gamma=1$$

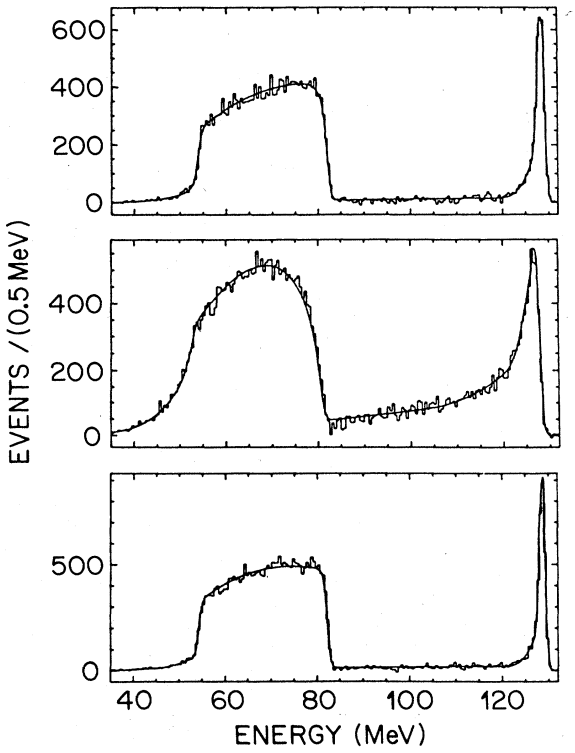

FIG. 3. Calibration spectra for the pair spectrometer from radiative pion capture in liquid hydrogen for different converters. Top: 2×88 μm gold, center: 600 μm lead, bottom: 176 μm gold. The upper line corresponds to the $\pi^-p\rightarrow n\gamma$ reaction, the continuum to the $\pi^-p\rightarrow n\pi^0$ reaction with subsequent decay of the π^0 into two photons. The solid line represents the results of the fit described in the text.

and

$$y_i=(E'_\gamma-\Delta E)^2/2\sigma_i^2\ ,$$

$$\sigma_i=R_i(E_\gamma-E_c)^{i/2}\ .$$

In this parametrization the average energy loss, which shifts the line to lower energies, is absorbed in the parameter ΔE. Three additional Gaussian functions with energy dependent width were used below the maximum to construct the low energy tail with a cutoff parameter E_c. For the acceptance function we used a Monte Carlo simulation as a starting point. It is based on the measured field map and allows the electron-positron pair to interact in the chambers and the converter foils. The energy dependence to the pair production cross section is taken into account, too. The relative acceptance was computed in 10 MeV steps and parametrized with a third order polynomial

$$A^{\rm MC}(E_\gamma)=\sum_{i=0}^{3}a_i(E_\gamma-E_A)^i\ .$$

The parameters are again given in Table I and the corresponding curves in Fig. 4. To consider also processes not properly simulated in the Monte Carlo program (see Ref. 21 for details), like interactions in the chamber gas and the helium bag and the difficulties in recognizing low

TABLE I. Parameters of the resolution function and the relative acceptance.

Converter	600 μm Pb	176 μm Au	2×88 μm Au
		Resolution	
ΔE (MeV)	−2.3±0.1	−0.77±0.02	−1.05±0.03
E_c (MeV)	22±2	39.5±0.7	28.4±0.5
C_0	1	1	1
C_1	3.6±1.0	0	0.30±0.05
C_2	1.7±0.4	0.22±0.03	0
C_3	1.3±0.3	0.029±0.001	0.029±0.002
R_0 (MeV)	0.78±0.04	0.62±0.01	0.72±0.02
R_1 (MeV$^{1/2}$)	0.23±0.02	0	0.27±0.02
R_2 (MeV)	0.080±0.009	0.027±0.001	0
R_3 (MeV$^{3/2}$)	0.034±0.003	0.058±0.002	0.039±0.001
		Acceptance	
$A_{abs}(E_\gamma=129.4$ MeV)	$(5.92\pm0.21)\times10^{-5}$	$(2.44\pm0.10)\times10^{-5}$	$(2.96\pm0.12)\times10^{-5}$
a_0	0.335	1.87	2.04
a_1 (MeV^{-1})	0.025	−0.018	−0.004
a_2 (MeV^{-2})	1.5×10^{-4}	-7.7×10^{-4}	-7.1×10^{-4}
a_3 (MeV^{-3})	-4.7×10^{-6}	-2.2×10^{-6}	-1.5×10^{-6}
a_4 (MeV^{-2})	$(7.4\pm0.5)\times10^{-5}$	$(3.7\pm0.2)\times10^{-5}$	$(5.4\pm0.2)\times10^{-5}$
E_A (MeV)	52.3	105.8	94.7

momentum tracks, which do not cross all chamber plans, we have allowed the acceptance to vary from the Monte Carlo values by introducing an additional factor into the fit

$$A^{\exp}(E_\gamma)=A^{\mathrm{MC}}(E_\gamma)[1-a_4(E_\gamma-129.4\ \mathrm{MeV})^2]\ .$$

The experimental acceptance deviated little from the predicted one, as apparent from Fig. 4. The measured acceptance is particularly well known in the region 55–83 MeV, which is also the region where most of the μ-capture events lie. The measured acceptance is used for the normalization, and the Monte Carlo simulation is only used as a starting point for the fit. Lastly the absolute acceptance at $E_\gamma=129.4$ MeV was determined by summing all events above 83 MeV, dividing by the number of pions stopping in the target ($f_{\mathrm{stop}}N_\pi$), the $\pi^-\mathrm{p}\to\mathrm{n}\gamma$ branching ratio (B), and correcting for photon absorption in the target and the events in the low energy tail below 83 MeV (f_T, typically 2%)

$$A_{\mathrm{abs}}=\frac{N_{\mathrm{rad}}}{N_\pi f_{\mathrm{stop}}}\frac{1}{B}f_T f_Q\ .$$

The factor f_Q (1.21) is needed, because the target-converter distance for the calibration runs was 85 cm rather than 78 cm as in the μ-capture measurements. Since the target size is small compared to the target-converter distance, the geometrical solid angle is independent of the stopping distribution. The absolute acceptances for the two converter configurations are $(2.96\pm0.12)\times10^{-5}$ (2×88 μm Au) and $(5.92\pm0.21)\times10^{-5}$ (600 μm Pb) plus $(2.44\pm0.10)\times10^{-5}$ (176 μm Au). They include solid angle, conversion efficiency, and detection efficiency.

C. Data reduction

After passing through a pattern recognition program, where the photon events were separated from the nonphoton triggers described in Sec. II B, the photon energy and direction were reconstructed from the chamber coordinates (see also Ref. 21). From the intersection of the photon direction with a vertical plane, which contains the muon beam center and the target, the nontarget associated background was determined. Figure 5 shows such a projection, with and without the Ca target in place. The photons which were created in the lead collimator edges could clearly be separated in space from the target photons. With a cut at 10 cm before and 15 cm behind the target nearly all unwanted photons were eliminated and only 1% of the good events were lost. Without the ^{40}Ca target less than 5% events came from the target region, which made extensive nontarget background runs unnecessary. The raw energy spectrum of those events surviving the target cut is shown in Fig. 6. We can distinguish three regions. For photon energies below 53 MeV ($m_\mu c^2/2$) the spectrum is dominated by muon decay events. Above 53 MeV and below 106 MeV ($m_\mu c^2$) we expect mainly radiative muon capture events. Above 106 MeV we find radiative pion capture events arising from the small pion contamination of the muon beam.

The muon decay events had two sources. Since the muon capture rate in Ca is $\Lambda_c=2.49\times10^6$ sec^{-1},[23–25] while the free muon decay rate is $\Lambda_{\mathrm{dec}}=4.54\times10^5$ sec^{-1}, 15.4±0.1% of all stopping muons decay. The radiative decay fraction $\mu^-\to\mathrm{e}^-\nu_e\nu_\mu\gamma$ was measured (1.4±0.4)% (Refs. 26 and 27) with a spectrum shape confirming the first order inner bremsstrahlung calculation.[28] Its contribution to the spectrum in our case is negligible, as indicated in Fig. 7. The main contribution came from the exter-

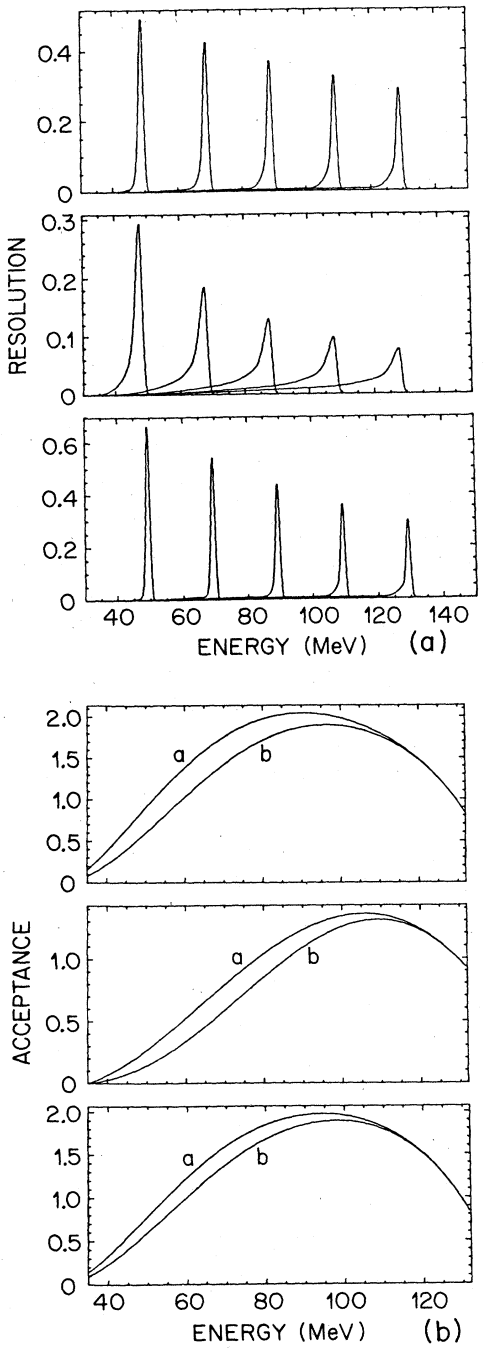

FIG. 4. Energy dependence of the pair spectrometer resolution (top) and acceptance (bottom). The three parts correspond to the three different converters used (see Fig. 3). The curves labeled a and b refer to the Monte Carlo prediction and the experimentally observed acceptance. The resolution curves are normalized to equal area, the acceptance is set equal to 1 at $E_\gamma = 130$ MeV.

nal bremsstrahlung produced by the decay electrons in the target. In Fig. 7 we show that the measured spectrum can be described well by folding the bound muon decay spectrum[29–31] with the bremmstrahlung's yield curve for a

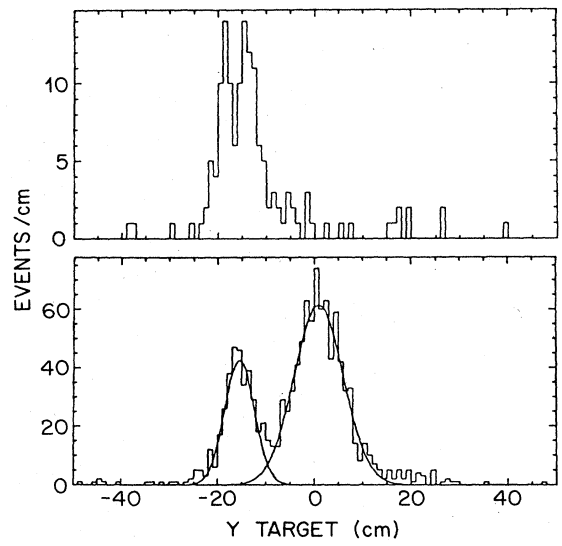

FIG. 5. Intersection of photon direction with the target plane. Upper peak: target events, lower peak: collimator events. Top: Background spectrum with target replaced by an empty target container.

target of 0.5 radiation length thickness (5.7 cm) (Ref. 32) and correcting for the energy variation of the acceptance and the average energy loss in the spectrometer. Above 57 MeV photon energy the decay events do no longer contribute. We therefore chose this energy as lower cutoff for the comparison with radiative muon capture calculations.

Since the radiative pion capture branching ratio[33] in Ca is 2% of all pion captures, a pion contamination of 10^{-3} suffices to produce a yield equal to that of radiative muon capture. The pion induced events can, however, be tagged, since they are all coincident with an incoming beam particle. Figure 8 shows such a prompt spectrum, where the photons appeared within a 20 nsec time window centered around the beam particle arrival time signaled by the last beam counter. It shows the expected enhancement of high energy photons, with a spectrum which agrees with the known radiative pion capture spectrum (Fig. 9) above 106 MeV. If we subtract this prompt spec-

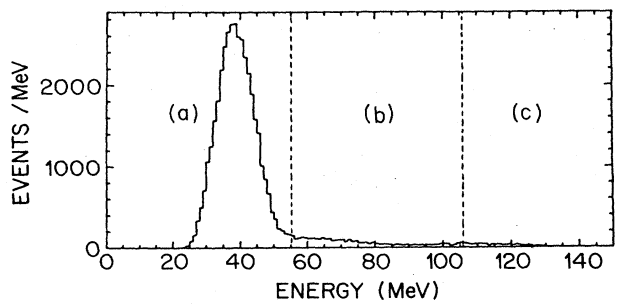

FIG. 6. Raw photon spectrum after target cut. (a), μ-decay bremsstrahlung; (b), radiative μ capture; (c), radiative π-capture energy regions.

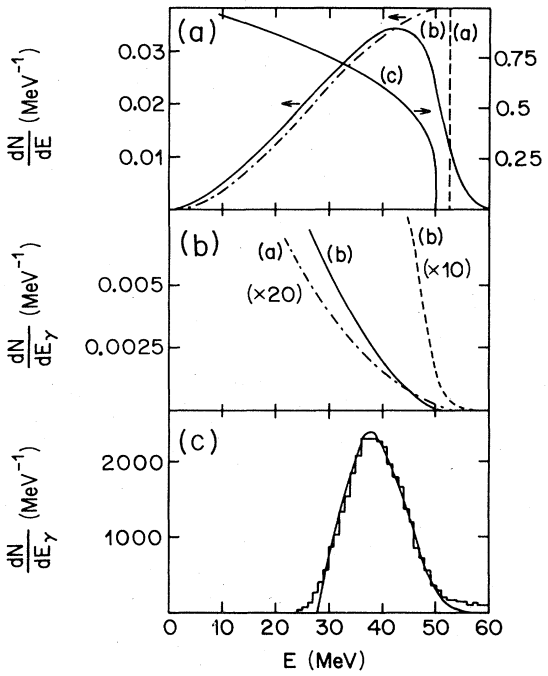

FIG. 7. (a): (a) Electron spectrum from free μ decay. (b) Electron spectrum from the decay of muons bound in ^{40}Ca (Ref. 31). (c) Bremsstrahlung yields $E_\gamma \cdot I(E_\gamma,t)t^{-1}$ for a target with thickness $t=0.5$ radiation length for an electron energy of 50 MeV (Ref. 32). (b): (a) Photon spectrum for radiative decay of free muons (Ref. 28). (b) External bremsstrahlungs spectrum for bound μ decay in ^{40}Ca (target thickness 0.5 radiation length) (c): Histogram: Experimental photon spectrum at low energies; curve: spectrum B,b multiplied with experimental acceptance and pair-spectrometer resolution.

trum from the total spectrum by cutting the events marked as prompt, we face two problems. Firstly the efficiency of the prompt tag is not 100%, such that some high-energy events are remaining after this cut, and secondly we also subtract those μ^--capture events occurring during the first 20 nsec of the μ^- lifetime (6%) as well as a contribution from a second μ^- appearing at random during this gate (6—10 %). The latter contribution can be obtained from the fraction (f_1) of μ-decay events

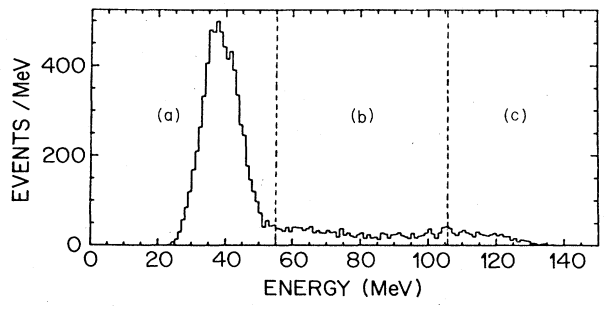

FIG. 8. Prompt photon spectrum (see text) (2×88 μm converter).

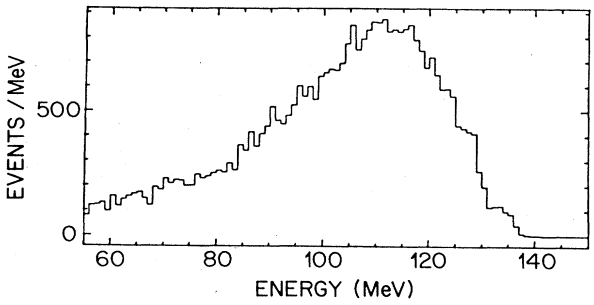

FIG. 9. Radiative pion capture photon spectrum (Ref. 33).

appearing with the prompt gate, while the former is measured by the fraction (f_3) of pion events after the prompt cut above $E_\gamma = m_\mu c^2$. We thus obtain

$$\frac{dN_\gamma(\mu^-,\nu_\mu\gamma)}{dE_\gamma} = \left[\frac{dN_\gamma^{\text{tot}}}{dE_\gamma} - \frac{dN_\gamma^{\text{prompt}}}{dE_\gamma}(1-f_3)^{-1}\right] \times[1-f_1/(1-f_3)]^{-1}\,.$$

This spectrum is shown in Fig. 10 for the 2×88 μm Au converter configuration, with which most of our data were taken, together with the raw spectrum. For this spectrum, e.g., the values of f_3 and f_1 are 0.292±0.014 and 0.140±0.002, respectively. The total pion contribution to the raw spectrum is 40% and 1600 radiative muon capture events remain after the subtraction. For the two other converter configurations we have after subtraction of the pion background 330 and 520 events, respectively.

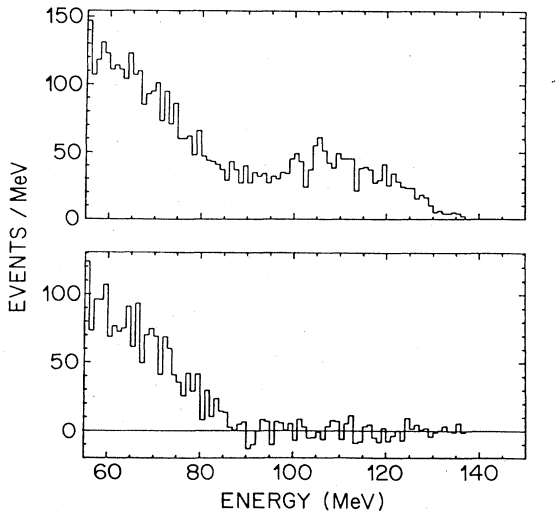

FIG. 10. Bottom: Radiative μ-capture spectrum (prompt events subtracted) (2×88 μm Au converter). Top: Raw photon spectrum (see text) (2×88 μm Au converter).

D. Normalization

To obtain the total radiative muon capture branching ratio and the normalized differential spectrum, we proceeded in the following way:

(i) The data sets from the converter configurations were treated separately to check their internal consistency.

(ii) The theoretical spectra from Christillin (C) (Ref. 16) and Rood, Yano, and Yano (RYY) (Ref. 11) were used for comparison with data and folded with the respective resolution and acceptance function for the three converters. The comparison to the RYY calculation is primarily made to be able to relate to the results of the latest previous experiment.[10]

(iii) For each spectrum a normalization factor (N_0) was used, defined by

$$N_0 = N_\mu (E_3 E_3^C)^{-1} f_{\text{stop}} (1 - f_{\text{dec}})(1 - f_{\text{abs}}) A_{\text{abs}} ,$$

where N_μ represents the number of incoming muons, E_3 represents the efficiency of beam scintillator μ_3 $=0.94\pm0.03$, E_3^C represents the counting losses caused by two muons appearing in the same beam burst $=0.95\pm0.03$, f_{stop} represents the fraction of muons stopping in the target, determined from range curves at low intensities $=0.79\pm0.04$, f_{dec} represents the muon decay fraction $=0.154\pm0.001$, f_{abs} represents the fraction of photons absorbed in the target $=0.16\pm0.03$, A_{abs} represents the absolute efficiency of the spectrometer at $E_\gamma = 129.4$ MeV (see Table I).

(iv) A fit to the data was made with the following expression:

$$S(E) = N_0 \int B(E') A_{\text{rel}}(E') R(E', E - E') dE' ,$$

with g_p(C, RYY) and the closure energy $k_{\max}$ (RYY) as only free parameters. The integrated rate is then taken from the theoretical spectrum. The variation of the photon absorption in the target with energy is less than 5%, thus $1 - f_{\text{abs}}$ varies only by less than 1%, which is why we applied this correction globally and did not include in the integral for $S(E)$. While the statistical errors (including the contributions from background uncertanties) of each data set were of course directly included into the least square fit, the errors on the normalization factors and the strongly correlated errors of the parameters of the resolution function and the relative acceptance need special treatment. We repeated the fit allowing all input parameters to vary by their standard deviation and thus determined the resulting contribution to the error in g_p and the total rate. The correlation between the acceptance and resolution parameters was taken into account using the error covariance matrix of the fit to the calibration spectra. Figure 11 shows the data sets used and the best fit curves obtained. The values for g_p and $k_{\max}$ as well as the total branching ratio above 57 MeV are given in Table II.

We refer to the discussion of the implications of these results for radiative μ-capture calculations in Sec. III. At this point we are only concerned with internal consistency of the three data sets. It is apparent from Table II that the branching ratios from all three data sets and the two theoretical models used as an ansatz for the spectral shape are in agreement with each other within their respective error bars. The data taken with the thicker converters, however, are statistically less significant.

E. Unfolded radiative muon capture spectrum

To facilitate comparison with the various other theoretical models available, for which the curves for different values of g_p were not made available to us, and future calculations we constructed an unfolded spectrum. This is fairly simple, since the resolution functions even for the thick converters are very narrow and the spectrum continuous and without strong or narrow features. We divided the measured spectra by the relative acceptance curve and the normalization factor and shifted the whole spectrum by the average energy loss appearing with each resolution function. Table III shows that fits to these unfolded spectra directly with the theoretical curves yield results consistent with the exact method. Finally now all three spectra can be combined into one spectrum with due consideration of statistical and normalization errors. We list this spectrum in Table IV and show it in Fig. 12 together with the two fits made to it. This spectrum represents the final result of our experiment and will be used below for comparison with existing models.

TABLE II. Consistency check for the three data sets taken with different converters. Results of a fit to the spectra after folding the theoretical curves with acceptance and resolution.

Converter	2×88 μm/Au	600 μm/Pb	176 μm/Au	Average
Christillin				
χ^2	55.9	53.3	47.5	
g_p/g_A	3.1 ±1.3	5.0±1.3	6.5±1.7	4.5 ±0.9
$B(E>57$ MeV$)(10^{-5})$	1.72±0.21	2.0±0.4	2.3±0.4	1.86±0.16
Rood-Yano-Yano				
χ^2	55.2	53.5	48.7	
g_p/g_A	1.0 ±1.1	4.8±3.4	6.6±2.6	2.2 ±1.0
$k_{\max}$ (MeV)	92.1 ±0.9	90.0±3.1	89.2±1.9	91.7 ±0.8
correlation	−0.784	−0.938	−0.912	
$B(E>57$ MeV$)(10^{-5})$	1.69±0.20	2.0±0.6	2.3±0.5	1.72±0.14

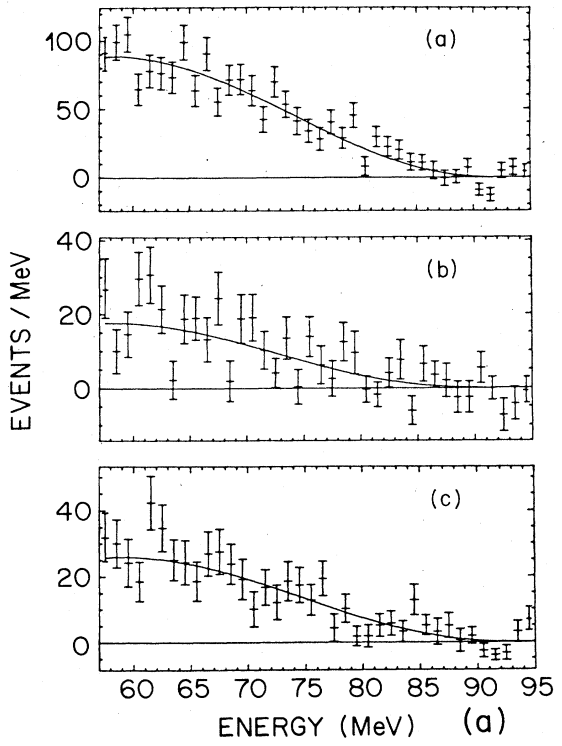

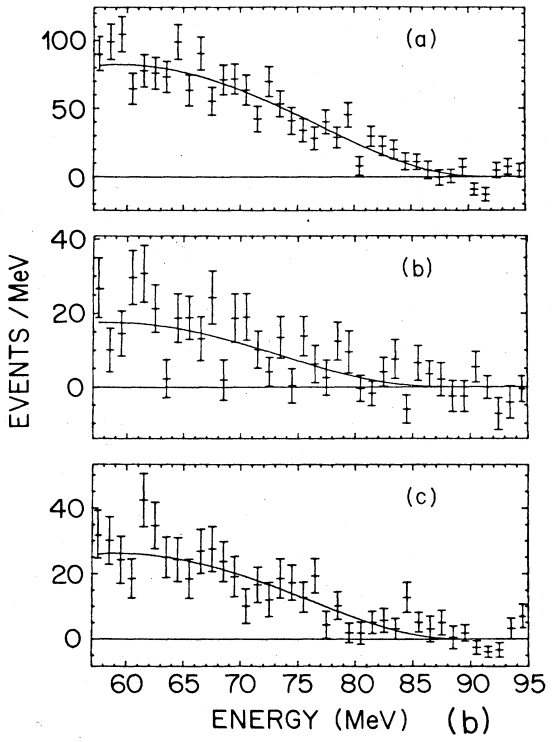

FIG. 11. Photon spectrum for $^{40}Ca(\mu^-,\nu_\mu\gamma)$ for three different converters: (a) 2×88 μm Au; (b) 600 μm Pb; (c) 176 μm Au. Bottom: Comparison with the Rood, Yano, and Yano calculation, top: Comparison with the theory of Christillin.

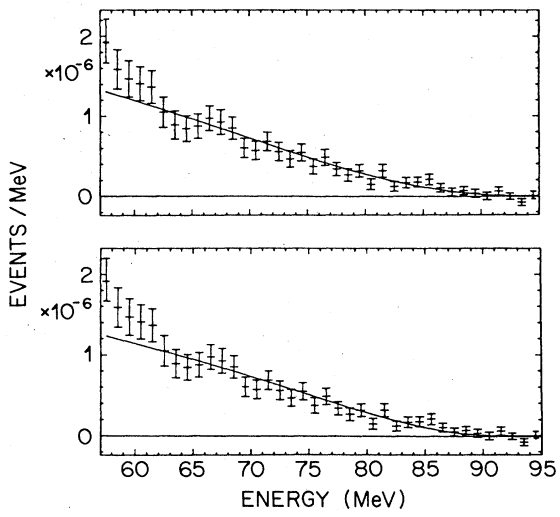

FIG. 12. Unfolded spectrum summed over all three converter configurations. Top: Theoretical curve of Christillin (Ref. 16). Bottom: Rood, Yano, and Yano (Ref. 11).

TABLE III. Results of fits to the unfolded spectra. Top: Each converter configuration treated individually. Bottom: Sum of all three spectra. The energy shift corresponds to the average energy loss at $E_\gamma=68$ MeV, the mean energy of the spectrum. (The numbers in the parentheses show the influence of the nonstatistical errors from the parameters of the acceptance function.)

Converter	2×88 μm/Au	600 μm/Pb	176 μm/Au
Energy shift (MeV)	2.2	6.4	1.8
Christillin			
χ^2	47	41	43
g_p/g_A	3.3 ±0.3	6.7 ±0.8	5.3 ±0.6
	(3.1 ±0.4)	(5.0±1.0)	(6.5±0.6)
$B(10^{-5})$	1.76±0.22	2.4±0.4	2.1±0.4
Rood-Yano-Yano			
χ^2	51	37	45
g_p/g_A	1.6 ±0.9	6.6±1.7	6.1±1.3
	(1.0 ±1.2)	(4.8±2.9)	(6.6±1.5)
k_{max} (MeV)	91.8 ±0.9	88.4±2.1	88.2±1.7
	(92.1 ±0.9)	(90.0±3.1)	(89.2±1.9)
$B(10^{-5})$	1.73±0.21	2.2±0.5	2.1±0.5
Christillin			
χ^2	49		
g_p/g_A	4.6 ±0.9		
$B(10^{-5})$	1.96±0.17		
Rood-Yano-Yano			
χ^2	60		
g_p/g_A	3.5 ±1.3		
k_{max}	90.8 ±0.9		
$B(10^{-5})$	1.92±0.20		

TABLE IV. Differential photon spectrum for $^{40}Ca(\mu^-,\nu_\mu\gamma)$ with resolution and acceptance unfolded. A ±9% uncertainty in the overall normalization is not included in the errors given for the individual points.

Energy (MeV)	dN_γ/dE_γ (10^{-6} MeV^{-1})	Energy (MeV)	dN_γ/dE_γ (10^{-6} MeV^{-1})	Energy (MeV)	dN_γ/dE_γ (10^{-6} MeV^{-1})
55.5	3.06±0.31	70.5	0.57±0.09	85.5	0.21±0.05
56.5	2.46±0.26	71.5	0.68±0.09	86.5	0.10±0.04
57.5	1.93±0.22	72.5	0.56±0.09	87.5	0.05±0.04
58.5	1.59±0.20	73.5	0.46±0.08	88.5	0.06±0.04
59.5	1.46±0.19	74.5	0.55±0.09	89.5	0.03±0.04
60.5	1.41±0.17	75.5	0.37±0.08	90.5	0.00±0.04
61.5	1.37±0.17	76.5	0.49±0.08	91.5	0.06±0.04
62.5	1.05±0.16	77.5	0.34±0.07	92.5	−0.01±0.04
63.5	0.89±0.14	78.5	0.26±0.06	93.5	−0.08±0.04
64.5	0.84±0.13	79.5	0.31±0.07	94.5	0.01±0.04
65.5	0.87±0.12	80.5	0.15±0.06	95.5	0.03±0.04
66.5	0.97±0.12	81.5	0.32±0.06	96.5	0.04±0.04
67.5	0.93±0.12	82.5	0.12±0.05	97.5	−0.03±0.04
68.5	0.85±0.11	83.5	0.17±0.05	98.5	−0.02±0.03
69.5	0.60±0.10	84.5	0.17±0.05	99.5	0.01±0.04

Summing all events above 57 MeV, we obtain a model independent radiative muon capture branching ratio of $\Lambda_\gamma(E_\gamma>57\ \text{MeV})/\Lambda_\mu=[2.07\pm0.06\ \text{(statistically)}\ \pm0.20\ \text{(including normalization)}]\times10^{-5}$. The uncertainty of our energy calibration (<200 keV) contributes an error $<2.4\%$ to this result.

This number is in good agreement with the result of Hart *et al.*,[10] who obtained $(2.11\pm0.14)\times10^{-5}$ by normalizing to muon decay with a bound muon lifetime of $\tau_\mu=(366\pm9)$ nsec, as determined in their experiment. This value is 8% higher than the average of the previous three experiments,[23–25] $\tau_\mu=(340\pm2)$ nsec. Using the latter value would reduce the branching ratio by 8%, but still not destroy the agreement. In our experiment we normalize to the number of captured muons and the muon lifetime enters only in the 15.4% decay correction. In the experiment of Hart *et al.*[10] the photon resolution is 29% FWHM at 130 MeV compared to our 1.5% FWHM and an ansatz using a polynomial in photon energy is needed to reconstruct an unfolded spectrum. The results of this final analysis also agree with a preliminary analysis based on part of our data,[34] which gave $\Lambda_\gamma/\Lambda_\mu=(2.0\pm0.4)\times10^{-5}$.

III. COMPARISON TO THEORETICAL CALCULATIONS AND DISCUSSION OF THE RESULTS

All theoretical calculations of radiative muon capture spectra for ^{40}Ca use the impulse approximation. They start with a nonrelativistic reduction of the amplitude for the elementary process $\mu^-p\to n\nu_\mu\gamma$, which is then used in the nuclear transition operator by summing over all nucleons. Beginning with the work of Rood and Tolhoek[3] several alternative methods for deriving these operators have been formulated (see, e.g., Refs. 35 and 36 for a discussion), which lead to consistent results up to terms linear in momentum transfer and photon momentum. The differences between the different predictions can therefore be traced solely to the different ways, in which the nuclear states are treated. As mentioned in the Introduction, only three calculations exist[16,18,19] which attempt a proper treatment of the nuclear response, while the majority employs the closure approximation in some form or another. We begin our comparison between experimental results and the calculations with the latter models, not only for historical reasons, but also to expose once again the inadequacy of these descriptions.

A. Closure models

In the closure calculations the sum over all final states contributing to the spectrum

$$\sum_f (k^{fi}_{\max}-k)^2\langle i\,|\,M^*\,|\,f\rangle\langle f\,|\,M\,|\,i\rangle$$

is replaced by

$$(k_{\max}-k)^2\langle i\,|\,M^*M\,|\,i\rangle\ ,$$

using the assumptions (k = photon energy)

$$k^{fi}_{\max}-k=m_\mu-\overline{\Delta E}-k=k_{\max}-k$$

and

$$\sum_f |f\rangle\langle f|=1\ .$$

The excitation energy of the final state E_f-E_i is replaced by an average value $\Delta\overline{E}$ with a corresponding end point of the photon spectrum $k_{\max}$. The impulse approximation transition operator M then needs to be evaluated only between the ^{40}Ca ground state wave functions, for which Rood and Tolhoek[3] have used harmonic oscillator shell-model wave functions. If the ordinary muon capture rate is evaluated in the same approximation the ratio of the two rates can be expressed in a simple way[3]

$$R(x)\sim \frac{k_{\max}^6}{\nu_{\rm av}^4} b_0(x)\left[1-2x+2x^2+\frac{1}{3}\frac{b_1(x)}{b_0(x)}x(1-x)\right]$$
$$\times x(1-x)^2 ,$$

where $x=k$(photon energy)$/k_{\max}$, $\nu_{\rm av}$ represents the neutrino momentum corresponding to the average nuclear excitation in ordinary capture, and $b_0(x),b_1(x)$ are functions containing the weak coupling constants. In the Primakoff[37] approximation, where only vector and axial-vector coupling are considered and only the radiation of the muon is retained with $k_{\max}=\nu_{\rm av}$, one obtains[3] $b_0=g_v^2+3g_A^2$ and $b_1=g_v^2-g_A^2$, i.e., $-\frac{1}{3}b_1/b_0\cong 0.03$. We show the corresponding spectrum, divided by the integrated rate and neglecting the term proportional to b_1 in Fig. 13. If one compares this simple result with the full calculations, containing all couplings and radiation from all charges and magnetic moments, one obtains a nearly identical curve, independent whether closure is applied with harmonic oscillator wave functions,[3] or whether the Fermi gas model[12] or a giant dipole resonance model[13] is used. For larger values of the induced pseudoscalar coupling more strength is shifted towards higher photon energies, but the slope in the experimentally accessible region is nearly not affected. Thus it is only the integrated rate above the experimental threshold which can be used to extract g_p. In first order the weak coupling constants enter into this rate as $g_v^2+3g_A^2+2g_pg_A\eta+g_p^2\eta^2$, with $\eta=m_\mu/2m_p$.[15]

In Sec. II we have presented a comparison of our data to one of the closure type models, the one of Rood, Yano, and Yano.[11] This calculation differs from the work of Rood and Tolhoek[3] primarily in the treatment of the muon propagator in the nuclear Coulomb field. While Rood and Tolhoek[3] use the free muon Green's function, the latter work solves for the Green's function in the field of an extended nucleus. The consequence of this is a typically 25% reduction of the rate for high photon energies. A good fit to the data is obtained for $g_p=(3.5\pm1.3)g_A$ and $k_{\max}=(90.8\pm0.9)$ MeV. This energy would correspond to an average excitation energy of the ^{40}K recoil of 11.8 MeV, and for the analog levels in ^{40}Ca at 19.4 MeV, quite close to the center of the giant dipole resonance. Hart *et al.* fit their spectrum with $k_{\max}=(86.3\pm1.8)$ MeV and $g_p=(6.7\pm1.5)g_A$. The larger value of g_p is simply a consequence of the lower value of $k_{\max}$, which is less well determined with 30% photon energy resolution, and reflects the k_m^6 dependence of the rate inherent of closure calculations.

Though the confidence level of the fit to the Rood-Yano-Yano theory is reasonable ($X^2=60$ for 36 degrees of freedom), the result has to be regarded with some caution, since an alternative investigation of the muon propagator nonlocality effects in several nuclei between ^{16}O and ^{208}Pb limits their influence to less than 10% on the high-energy part of the spectrum.[17] With a smaller renormalization our experimental rate would then lead to negative values of g_p/g_A, as the comparison with all other closure models requires. In Figs. 14 and 15 we compare our spectrum to these calculations. Fearing[13] relates the radiative muon

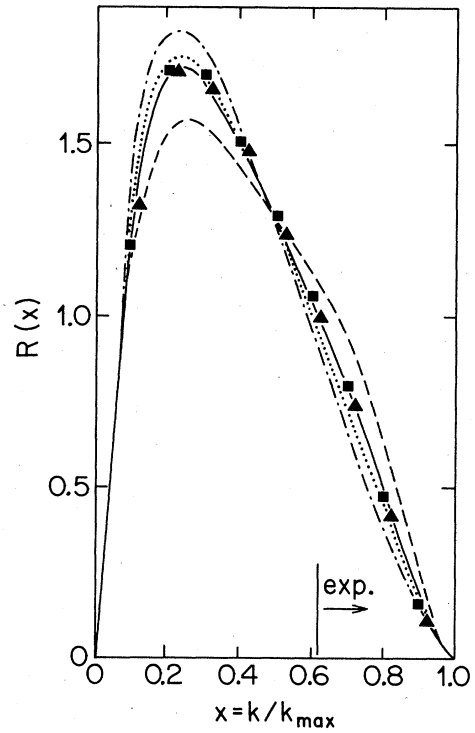

FIG. 13. Radiative muon capture photon spectrum in the closure approximation. Plotted are the normalized spectra $(\int R(x)dx)^{-1}R(x)$ with $x=k/k_{\max}$, the photon energy relative to its maximum value. The solid curve corresponds to $g_p=8g_A$, while the dashed and dashed-dotted curves correspond to $g_p=0$ and $g_p=16g_A$, respectively (calculations of Ref. 3). The squares and triangles represent the results of Refs. 12 and 13, respectively. The region covered by experiments starts near $x\cong 0.6$. The dotted curve corresponds to $R(x)=20(1-2x+2x^2)x(1-x)^2$, the Primakoff approximation (see text).

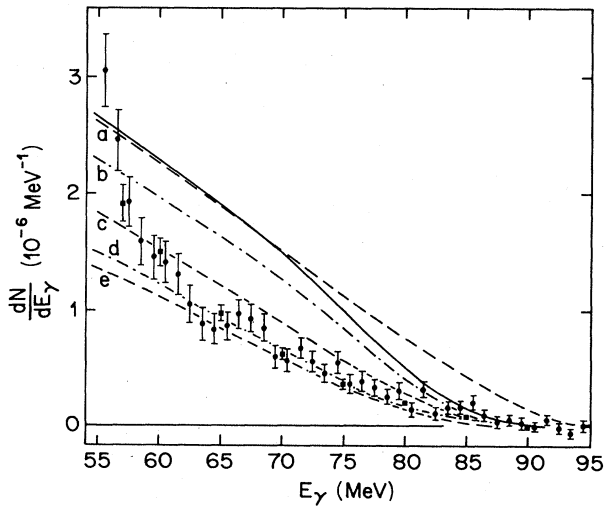

FIG. 14. Comparison of experimental results to closure-type calculations. Solid curve: Borchi and Gennaro (Ref. 12); $g_p=9g_A$; $k_{\max}=90.5$ MeV. Dashed curves: Fearing (Ref. 13); (a) $g_p=10g_A$, (c) $g_p=7g_A$, (d) $g_p=4g_A$, $k_{\max}=88$ MeV. Dashed-dotted curves: Fearing (Ref. 13); (a) $k_{\max}=96$ MeV, (e) $k_{\max}=80$ MeV, $g_p=7g_A$.

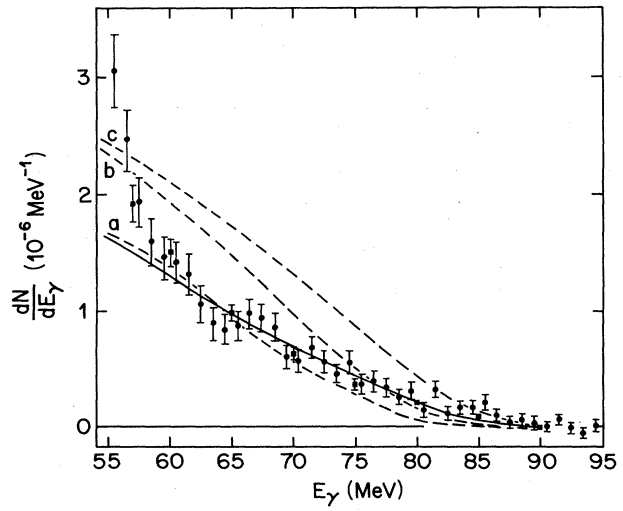

FIG. 15. Comparison of experimental results to the calculations of Sloboda and Fearing (Ref. 14). Dashed curves: (a) $g_p=0$, (b) $g_p=7g_A$ (closure; harmonic oscillator), (c) $g_p=7g_A$ (giant dipole model), $k_{max}=87.6$ MeV. Solid curve: Best fit to the experimental results of Ref. 10 (see text).

capture strength into giant dipole states to the experimental strength, observed in photonuclear reactions. Since the higher multipoles, especially the quadrupole strength, are evaluated with harmonic oscillator wave functions, but with the excitation energy coinciding with the giant dipole resonance, this amounts essentially again to the closure approximation as Fig. 13 demonstrated. Though our value of k_{max} seems to be consistent with the assumption of the concentration of strength into giant dipole states,

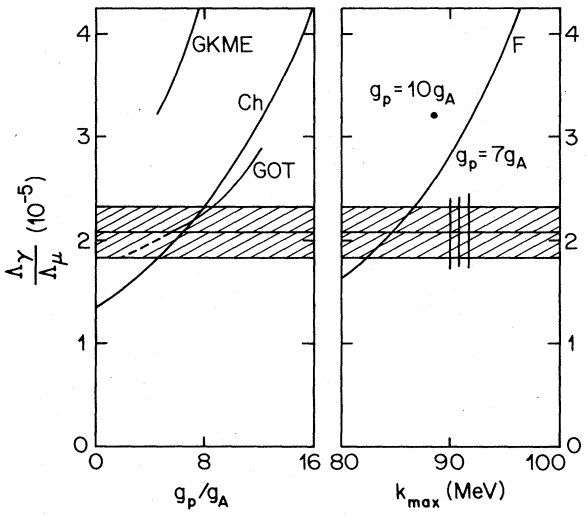

FIG. 16. Left: Comparison of the experimental rate Λ_γ ($E_\gamma \geq 57$ MeV)/Λ_μ^{tot} to the calculations of Gmitro *et al.* [GMKE (Ref. 18), GOT (Ref. 19), and Christillin (Ref. 16)] versus g_p/g_A. Right: Comparison of the experimental rate to the calculations of Fearing (Ref. 13) versus k_{max}. The vertical lines indicate the value of k_{max} found in our experiment.

the rate computed in this model exceeds the experimental one for all positive values of g_p/g_A. An improved version of this model presented by Sloboda and Fearing[14] considers also terms of order m_p^{-2}, which are missing in the other calculations. These results are displayed in Fig. 15. The best fit to spectrum of Hart *et al.* yielded $k_{max}=(89.1\pm0.9)$ MeV and $g_p=(-2.8\pm4.8)g_A$ in the closure harmonic oscillator model and $k_{max}=(87.0\pm3.0)$ MeV and $g_p=(-0.3\pm2.0)g_A$. Our data with a higher k_{max}, but similar rate, would yield even lower values of g_p (see Fig. 16).

Lastly, the combination of the Fermi-gas model and closure, used by Borchi and Gennaro,[12] gives results (Fig. 14) which exceed the experiment by more than a factor of 2 for $g_p=8g_A$, which again requires g_p/g_A less than zero, bearing in mind the combination of coupling constants entering the rate, which we referred to above.

B. Phenomenological response function

Christillin,[16] whose criticism of the closure approximation we have reproduced in the Introduction, has introduced a nuclear response function, which divides the transition strength into a dipole and a quadrupole part. The dipole resonance is taken at 20 MeV excitation energy with a Lorentzian width of 5 MeV, the quadrupole resonance at 35 MeV with a width of 12 MeV. The dependence of the momentum transfer is incorporated by multiplying the strength with the square of the elastic form factor of the ^{40}Ca ground state. The strength of the quadrupole part is adjusted to reproduce the rate for ordinary muon capture, the dipole part can be related to photoabsorption data assuming SU(4) invariance. With such a phenomenological response function the range of excitation energies accessible for each photon energy is properly accounted for, at energies higher than 75 MeV essentially only the giant dipole resonance contributes, while below 75 MeV both parts are present. When compared to closure models a considerable reduction of the rate is obtained. The overall fit of this model to our data was presented in Sec. II. The only free parameter is now g_p. The fit gives $X^2=49$ for 37 degree of freedom with $g_p=(4.6\pm0.9)g_A$, which corresponds to (68 ± 13) % of the canonical value. Since the fit stays below the experimental points for the energies below 61 MeV, which make a comparatively large contribution to the total rate, matching the summed experimental rate above 57 MeV to the predicted rate (see Fig. 16) tends to give slightly higher values of g_p.

C. Microscopic calculation

The ideal procedure, from a theoretical point of view, to compute the spectrum would be to sum over all possible partial transitions, taken at their correct energies using wave functions, which have been well tested against other processes with similar one-body matrix elements such as electron scattering, photonuclear reactions, radiative pion capture, etc. For ^{40}Ca such a program is clearly too ambitious, though it has been attempted for ^{16}O.[18] However, microscopic calculations for ^{40}Ca with simple shell-model wave functions[38] assuming ^{40}Ca doubly closed and includ-

ing all negative 1p-1h states have been carried out.[18] We display the results as a function of g_p in Fig. 16. The rate is clearly overestimated.

This problem has been remedied recently. Gmitro and Ovchinnikova[39] have constructed an improved impulse approximation Hamiltonian, which ensures the continuity of the nuclear electromagnetic current (Siegert's theorem) and is viewed as an implicit calculation of the meson exchange current at the electromagnetic vertex. When this Hamiltonian is used for ^{40}Ca (Ref. 19) a dramatic reduction of the yield is obtained. With a value of $g_p=(5.8\pm2.4)g_A$ the rate is in agreement with the experimental one (see Fig. 16). Two reservations have to be made with respect to this result, as pointed out in Ref. 19. The quadrupole branch is not included in the ordinary as well as in the radiative muon capture rate due to computational difficulties. While the contributions of the quadrupole branch to radiative capture are small, because of the available phase space at high photon energies, they can contribute up to 30% the ordinary muon capture[40] and thus affect the ratio. Gmitro *et al.*[19] have therefore multiplied their ordinary muon capture rate by a correction factor 1.3. Furthermore nucleon velocity terms in the Hamiltonian are dropped, which, however, affect both rates by typically 10% and are therefore unimportant. The last comment pertains to the shape of the spectrum. Again the theoretical curves (see Fig. 17) fall below the experimental ones at low photon energies, where the contribution to the integrated rate is large and precisely where the quadrupole branch should rise. Consequently a fit to the spectrum requires a value for g_p lower than quoted above. Extrapolating from the curves given for $g_p=7.5g_A$ and $g_p=4g_A$ we would obtain a good fit with $g_p=(3.0\pm0.6)g_A$. These results bring the microscopic calculations in complete agreement with the phenomenological ansatz.

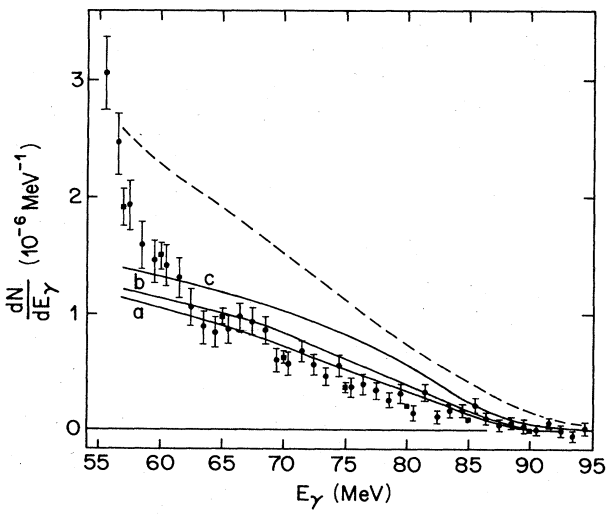

FIG. 17. Comparison of the experimental spectrum to the shell-model calculations of Gmitro *et al.* (Refs. 18 and 19). Dashed curve: No continuity constraints applied, $g_p=7.5g_A$ (Ref. 18). Solid curves: Continuity constraints included: (a) $g_p=4.5g_A$, (b) $g_p=7.5g_A$, (c) $g_p=12g_A$.

D. Conclusions

We have observed that our experimental results can be explained satisfactorily with two realistic, in the sense of treating the nuclear response, model calculations, if the size of the induced pseudoscalar coupling at the momentum transfer for ordinary muon capture in hydrogen is taken within the range $g_p=(4.0\pm1.5)g_A$ [combining the results of the fits to the spectra $g_p=(3.0\pm0.6)g_A$, Sec. III B and $g_p=(4.6\pm0.9)g_A$, Sec. III C]. This value corresponds to (59±22) % of the partial conservation of axial-vector current (PCAC) value of $6.78g_A$ and to (57±25) % of what is measured in ordinary muon capture, and thus indicates considerable quenching of this coupling in nuclei.

The renormalization of the axial weak couplings has been the subject of several theoretical investigations.[41–43] In particular the induced pseudoscalar coupling, which arises from the exchange of a virtual pion, is expected to be most sensitive to alterations of the pion field in the nuclear medium. The intermediate pion may interact with other nucleons and the emitting nucleon may be affected by short range correlations. The axial polarizability parameter α characterizes the former, the screening parameter ξ the latter effect. If the pion field, coupling to an isolated nucleon, may be obtained as

$$(-\nabla^2+m_\pi^2)\phi_\pi(x)=-\frac{g_r}{2m_\pi}\nabla\sigma(x)\ ,$$

the field in the presence of other nucleons is written as

$$[-\nabla(1+\alpha)\nabla+m_\pi^2]\phi(x)=-\frac{g_r}{2m_N}\nabla(1+\tfrac{1}{3}\xi\alpha)\sigma(x)\ .$$

The left-hand side of this equation leads to replacement of the pion mass in the propagator by an effective mass $m_{\pi'}^2=m_\pi^2(1+\alpha)^{-1}$, while the modification of the strong coupling on the right-hand side leads to a renormalization of both axial-vector and induced pseudoscalar coupling by the factor $(1+\frac{1}{3}\xi\alpha)$:

$$g_A^{\rm eff}=g_A(1+\tfrac{1}{3}\xi\alpha)\ ,$$

$$g_p^{\rm eff}=g_p(1+\tfrac{1}{3}\xi\alpha)\frac{-q^2+m_\pi^2}{-q^2+m_{\pi'}^{12}}\ .$$

In this framework we are measuring in our experiment ($q^2=-0.88m_\mu^2$)

$$\left[\frac{g_p}{g_A}\right]^{\rm eff}\Big/\left[\frac{g_p}{g_A}\right]^{\rm hydrogen}=\frac{-q^2+m_\pi^2}{-q^2+m_{\pi'}^{12}}=0.57\pm0.25\ .$$

Solving for α we obtain $\alpha=-0.53\pm0.25$. The value expected for nuclear matter is $\alpha=-0.75$.

These findings are contradicted by the unrenormalized values of g_p found for partial transitions in ^{16}O (Ref. 15) and ^{12}C.[6] It has been argued[44] that the renormalization in these peripheral transitions of valence nucleons should be smaller than in the heavier and larger ^{40}Ca system. Explicit calculations of meson exchange current contributions to the renormalization of the weak vertex parameters for radiative muon capture in ^{40}Ca indicate that a downward renormalization of g_p and a consequent reduction of the

rate is indeed expected. Ohta[45] finds a 30% reduction of the rate compared to Rood and Tolhoek,[3] while Achmedov *et al.*[46] find typically 10% compared to the impulse approximation calculated performed with shell model wave functions. The latter result is nearly independent of the parameter ξ, but even with meson exchange currents included the predicted rate exceeds the experimental rate by a factor of 2, rather similar to the results discussed in Sec. III C without the continuity constraint on the electromagnetic vertex.

In view of the many uncertainties inherent to extraction of g_p from the inclusive photon spectrum, our conclusions regarding the quenching of induced pseudoscalar coupling cannot be considered final. There is certainly room for further improvements of the calculations, e.g., the inclusion of positive parity states (quadrupole excitations), the inclusion of ground state correlations ($2\hbar\omega$ admixtures to the ^{40}Ca ground state), etc. There is also hope that the measurements of the photon-muon spin angular correlation, which have been attempted[10,47–49] but so far only yielded inconclusive results, can be sufficiently improved to allow a redetermination of g_p to an accuracy around 10 to 20%. The photon-muon spin angular correlation parameter is strongly dependent on g_p, too, but seems to depend only weakly on the choice of the nuclear model, as an inspection of all calculations cited above shows. Such measurements are in progress at TRIUMF (Ref. 49) and at SIN.[50]

ACKNOWLEDGMENTS

We thank Dr. M. Gmitro and Dr. P. Christillin for numerous discussions on radiative muon capture calculations and Prof. H. P. C. Rood for making available his compute code, which allowed the comparison with the computations of Ref. 11. The experiment was strongly supported by Prof. J. P. Blaser and his SIN crew. Further support was received from the Swiss and German funding agencies for basic research, "Schweizerischer Nationalfond" and "Deutsche Forschungsgemeinschaft."

*Present address: Kernkraftwerk Leibstadt AG, CH-4353 Leibstadt, Switzerland.

†Present address: Institut für Astronomie, ETH, CH-8092 Zürich, Switzerland.

‡Present address: IABG, D-8021 Ottobrunn, Federal Republic of Germany.

§Present address: NAGRA, CH-5401 Baden, Switzerland.

**Present address: McKinsey Co. Inc., D-8000 München, Federal Republic of Germany.

[1]N. C. Mukhopadhyay, Phys. Rep. **30C**, 1 (1977).

[2]S. K. Manacher and L. Wolfenstein, Phys. Rev. **116**, 782 (1959).

[3]H. P. C. Rood and H. A. Tolhoek, Nucl. Phys. **70**, 658 (1965).

[4]G. Bardin *et al.*, Phys. Lett. **104B**, 320 (1981).

[5]C. A. Gagliardi *et al.*, Phys. Rev. Lett. **34**, 212 (1975).

[6]L. Ph. Roesch *et al.*, Helv. Phys. Acta **55**, 74 (1982); Phys. Lett. **B107**, L31 (1981); Phys. Rev. Lett. **46**, 1507 (1981).

[7]L. Wolfenstein, in *High-Energy Physics and Nuclear Structure,* edited by S. Devons (Plenum, New York, 1970), p. 661.

[8]M. Conversi, R. Diebold, and L. di Lella, Phys. Rev. **136**, B1077 (1964).

[9]L. M. Rosenstein and J. M. Hammerman, Phys. Rev. C **8**, 603 (1973).

[10]R. D. Hart *et al.*, Phys. Rev. Lett. **39**, 399 (1977).

[11]H. P. C. Rood, A. F. Yano, and F. B. Yano, Nucl. Phys. **A228**, 333 (1974); Phys. Lett. **35B**, 59 (1971); **37B**, 189 (1971).

[12]E. Borchi and R. Gatto, Nuovo Cimento **33**, 1472 (1964); E. Borchi and S. de Gennaro, Phys. Rev. C **2**, 1012 (1972).

[13]H. W. Fearing, Phys. Rev. **146**, 723 (1966).

[14]R. S. Sloboda and H. W. Fearing, Phys. Rev. C **18**, 2265 (1978); Nucl. Phys. **A340**, 342 (1980).

[15]P. Christillin, M. Rosa-Clot, and S. Servadio, Nucl. Phys. **A345**, 331 (1980); Phys. Lett. **73B**, 23 (1978).

[16]P. Christillin, Nucl. Phys. **A362**, 391 (1981); Czech. J. Phys. **B32**, 266 (1982).

[17]P. Christillin, M. Rosa-Clot, and S. Servadio, Nucl. Phys. **A345**, 317 (1980).

[18]M. Gmitro *et al.*, Czech. J. Phys. **B31**, 499 (1981).

[19]M. Gmitro, A. A. Ovchinnikova, and T. V. Tetereva, Joint Institute for Nuclear Research (Dubna) report, 1984.

[20]SIN Users Handbook (1981), p. 37.

[21]J. C. Alder *et al.*, Nucl. Instrum. Methods **160**, 93 (1979).

[22]J. Spuller *et al.*, Phys. Lett. **67B**, 479 (1977).

[23]J. C. Sens, Phys. Rev. **113**, 679 (1959).

[24]W. R. Cramer, Nuovo Cimento **24**, 546 (1962).

[25]L. di Lella, I. Hammerman, and L. M. Rosenstein, Phys. Rev. Lett. **27**, 830 (1971).

[26]E. Bogart *et al.*, Phys. Rev. **156**, 1405 (1967).

[27]W. Eichenberger, A. van der Schaaf, and R. Engfer, Nucl. Phys. **A412**, 523 (1984).

[28]R. R. Crittenden *et al.*, Phys. Rev. **121**, 1823 (1961).

[29]R. Hänggi *et al.*, Phys. Lett. **51B**, 119 (1974).

[30]R. W. Huff, Ann. Phys. (N.Y.) **16**, 288 (1961).

[31]R. Herzog, private communication.

[32]Y. S. Tsai and V. Whitis, Phys. Rev. **149**, 1248 (1966).

[33]J. C. Alder *et al.*, *Photopion Nuclear Physics,* edited by P. Stoler (Plenum, New York, 1978), p. 107.

[34]A. Frischknecht *et al.*, Czech. J. Phys. **B32**, 270 (1982).

[35]M. Gmitro and A. A. Ovchinnikova, Nucl. Phys. **A356**, 323 (1981).

[36]P. Christillin and S. Servadio, Nuovo Cimento **42**, 165 (1977).

[37]H. Primakoff, Rev. Mod. Phys. **31**, 802 (1959).

[38]T. W. Donelly and G. E. Walker, Ann. Phys. (N.Y.) **60**, 209 (1970).

[39]M. Gmitro and A. A. Ovchinnikova, Joint Institute of Nuclear Research (Dubna) report, 1984; Proceedings of the Xth International Conference on Particles and Nuclei, Heidelberg, 1984, Vol. I, p. A65.

[40]Nguyen van Gai, N. Auerbach, and A. Z. Mekjian, Phys. Rev. Lett. **46**, 1444 (1981).

[41]M. Ericson, Prog. Part. Nucl. Phys. **1**, 67 (1978).

[42]M. Ericson, in *Mesons in Nuclei,* edited by M. Rho and D. Wilkinson (North-Holland, Amsterdam, 1979), Vol. III, p. 905.

[43]J. Delorme, M. Ericson, A. Figureau, and C. Thevenet, Ann. Phys. (N.Y.) **102**, 273 (1976).

[44]J. Deutsch, Proceedings of the TRIUMF Muon-Physics Facility Workship, 1980, TRIUMF Report TR I-81, 1981, p. 1.
[45]K. Ohta, Phys. Rev. Lett. **33**, 1507 (1974).
[46]E. C. Achmedov, R. A. Eramzhyan, and T. V. Tetereva, Institute for Nuclear Research, Academy of Sciences (USSR), Report P-0368, 1984.
[47]L. di Lella, I. Hammerman, and L. M. Rosenstein, Phys. Rev. Lett. **27**, 830 (1971).
[48]A. Frischknecht *et al.*, Helv. Phys. Acta **53**, 647 (1980).
[49]M. D. Hasinoff *et al.*, in Proceedings of the Xth International Conference on Particles and Nuclei; Heidelberg, 1984, Vol. II, p. H4.
[50]M. Doebeli *et al.*, in Proceedings of the Xth International Conference on Particles and Nuclei; Heidelberg, 1984, Vol. II, p. H2.